Materials Science & Engineering C 111 (2020) 110802

Contents lists available at ScienceDirect

Materials Science & Engineering C

journal homepage: www.elsevier.com/locate/msec

Dissolution activation energy of a fluorapatite glass-ceramic veneer for dental applications

S.M. Hsu[a,*], F. Ren[b], C. Batich[c], A.E. Clark[d], V. Craciun[e,f], J.F. Esquivel-Upshaw[g]

[a] Restorative Dental Sciences, Division of Prosthodontics, University of Florida, Gainesville, FL, USA
[b] Department of Chemical Engineering, University of Florida, Gainesville, FL, USA
[c] Department of Material Science and Engineering, University of Florida, Gainesville, FL, USA
[d] Restorative Dental Sciences, Division of Prosthodontics, University of Florida, Gainesville, FL, USA
[e] National Institute for Lasers, Plasma and Radiation Physics, Magurele, Ilfov, Romania
[f] DENTIX MILLENNIUM SRL, Sabareni, Giurgiu, Romania
[g] Restorative Dental Sciences, Division of Prosthodontics, University of Florida, Gainesville, FL, USA

1. Introduction

A chemical reaction is a process where reactants are transformed into products. In order for a reaction to occur, reactant molecules need to be in proximity with each other and there needs to be sufficient energy to overcome the energy barrier. This energy is called activation energy (Ea). Several researchers have studied the materials' activation energies for different chemical reactions. For the hydrolysis reaction involved in the dissolution of quartz and amorphous silica in water, the Ea was found to be in the range of 60.9 to 76.6 kJ/mol [1]. Mazer and Walther investigated the temperature dependence of vitreous silica dissolution at pH 4.1 and reported Ea to be 95 kJ/mol [2]. Maraghechi et al. studied the dissolution and precipitation reactions of amorphous silica at high pH aqueous solution and dissolution Ea was calculated as 87.5 kJ/mol [3]. These high values indicate that breaking the bond between silicon and oxygen is the rate-limiting step to this reaction [1].

Fluorapatite glass-ceramic veneer is used as a dental restorative material [4]. The corrosion of glass-ceramic is dominated by two main reactions [5,6] depending on the pH of the environment. There is total dissolution with a breakdown of the silica network in an alkaline solution and an ionic exchange process between alkalis of glass-ceramic and protons in acidic conditions.

Chemical durability is one of the most important criteria for dental materials as this represents resistance to surface degradation in the presence of environmental pH [7–11] changes, since the oral cavity can be a hostile chemical environment to dental restorative materials. Dental ceramics will eventually undergo degradation resulting from mechanical occlusion, chemical corrosion, or a combination of both [12]. Corrosion can lead to decreased fracture strength [13] and surface roughness, which will eventually lead to abrasive wear and accumulation of plaque on the surface of teeth. Štefančić et al. reported that the surface roughness of glazed yttria partially stabilized tetragonal zirconia dental ceramic increased after corrosion in acid [14]. The increased surface roughness of antagonistic ceramic is unfavorable for enamel wear [15], and can result in more plaque accumulation on rougher surfaces, which can in turn, promote tooth decay [16,17].

Prediction of clinical performance for dental materials is the essence of testing methodologies. In vitro testing needs to be realistic, expedient and financially viable. As such, accelerated testing at higher temperatures has been employed to allow several years worth of degradation to occur in a significantly shorter amount of time. However, employing elevated temperatures can elicit other chemical reactions, which would not normally occur at regular body temperatures (37 °C for intraoral temperatures).

Since glass-ceramic consists of oxides, a thorough understanding of the compounds, which play a role in corrosion in different solutions, is needed. However, previous studies have mainly focused on the corrosion and Ea of silica [1–3,18]. The aim of this study was to determine the activation energy of the dissolution kinetics of a fluorapatite glass-ceramic veneer in alkaline and acidic conditions as a function of dissolution rate at different temperatures to justify their predictability under clinical conditions.

2. Materials and methods

2.1. Specimens preparation

Fluorapatite glass-ceramic veneers (Zirpress, Ivoclar Vivadent AG, Schaan, Liechtenstein) were cut into 12 × 1.2 ± 0.4 mm disks and polished using a grinder-polisher (EcoMet™ 250 AutoMet™ 250 Power Head, Buehler) with 340, 400 and 600 grits of silicon carbide abrasive paper (Carbimet, Buehler) on both sides of the disks. The disks were

* Corresponding author at: University of Florida, College of Dentistry, Restorative Dental Sciences Department, 1395 Center Drive, Rm D9-6, Gainesville, FL 32610, USA.
E-mail addresses: shuminhsu@ufl.edu (S.M. Hsu), fren@che.ufl.edu (F. Ren), cbati@mse.ufl.edu (C. Batich), BCLARK@dental.ufl.edu (A.E. Clark), valentin.craciun@inflpr.ro (V. Craciun), JESQUIVEL@dental.ufl.edu (J.F. Esquivel-Upshaw).

https://doi.org/10.1016/j.msec.2020.110802
Received 29 August 2019; Received in revised form 8 November 2019; Accepted 29 February 2020
Available online 05 March 2020

Table 1
The compositions (wt% and atomic %) of the glass-ceramic used in this study [19].

Composition	SiO_2	Al_2O_3	Na_2O	K_2O	CaO	ZnO	ZrO_2	P_2O_5	F	Other oxides	Pigments
wt%	57.0–62.0	12.0–16.0	7.0–10.0	6.0–8.0	2.0–4.0		1.5–2.5	1.0–2.0	0.5–1.0	0–6.0	0.2–0.9
atomic%	58.6–51.6	14.5–15.7	13.9–16.1	7.8–8.5	2.2–3.5		0.7–1.0	0.4–0.7	1.6–2.6		

cleaned with ethanol under ultrasonication (Pro-Sonic 600, Sultan) and rinsed with deionized distilled water. The composition of fluorapatite glass-ceramic disks (IPS e.max ZirPress scientific documentation, Ivoclar Vivadent) is listed in Table 1.

2.2. Experimental design

The disks were dried in the oven at 100 °C to 105 °C for 24 h and cooled in the desiccator before weight measurement. The measurement was performed prior to and after corrosion experiments with an accuracy of 0.1 mg (AS60/220.R2 Analytical balance, RADWAG). The corrosion experiments were performed at (i) different immersion days; for 3, 15, and 30 days at 85 °C, and (ii) different temperatures; 37, 55, 65, 75 and 85 °C for 30 days. The disks were immersed in 15 ml of pH 10 (Ammonium chloride-ammonium hydroxide buffer solution, Sigma-Aldrich), pH 7 (mixture of 0.1 M tris (hydroxymethyl) aminomethane and 0.1 M HCl), and pH 2 (glycine buffer solution, Santa Cruz Biotechnology, Inc.). Five disks were used for each condition per group. All disks were placed in polyethylene centrifuge tubes (Thermo Scientific Nalgene Oak Ridge High-Speed Centrifuge Tubes, Thermo Fisher Scientific) and a shaking water bath (TSBS40, Techne USA) with 50 oscillations per minute. After corrosion for 30 days, the amount of released K, Na, Ca, Si, Al, and Zn ions in the solution were analyzed by inductively coupled plasma atomic emission spectrometer (ICP, 3200RL, PerkinElmer).

2.3. Surface characterization

2.3.1. X-ray diffraction analysis

X-ray diffraction was used to analyze fluorapatite glass-ceramic disks before (as reference) and after corrosion. The X-ray diffraction investigations were performed with an Empyrean instrument (Panalytical, The Netherlands). The instrument works with a Cu anode (Cu Kα radiation) at a power of 45 kV and 40 mA. For symmetrical XRD investigations, the instrument was set up in a Bragg-Brentano geometry with a 1/2° slit and a 0.04 rad Soller slit in the incidence beam side and a 1° receiving slit, a 0.04 rad large Soller slit, a Ni β filter and a 1 D Pixcell detector in the diffracted beam side. In this geometry, X-rays penetrate tens of micrometers, so the estimated phase composition corresponds to bulk.

The grazing incidence X-ray diffraction geometry was performed in a parallel X-ray beam geometry, which limits the analyzed volume to the outermost surface region of the sample. In this case, an X-ray mirror and a 1/8° slit was used in the incident beam side and a 0.27° thin film collimator on the diffracted beam side. After careful alignment, an incidence angle of 0.1° was chosen, which limits the analyzed depth to around 100 nm, up to a maximum of 200 nm. A more exact estimation of the penetration depth could not be performed because of the rather rough surface of chemically treated samples. The 2018 ICCD powder diffraction database was used to analyze the acquired patterns.

2.3.2. X-ray photoelectron spectroscopy analysis

The surface compositions of disks before corrosion (as reference) and after corrosion were analyzed in a ULVAC-PHI XPS instrument with Al monochromatised Kα radiation from a 50 W X-ray source. Survey scans were recorded in the range 0–1100 eV binding energy with a 0.8 eV step size.

2.3.3. Scanning electron microscopy analysis

The morphologies of the disks were examined by scanning electron microscopy (Phenom Desktop SEM, Thermo Scientific). The images were obtained at 5 kV before corrosion (as reference) and after corrosion in pH 10 and pH 2.

2.3.4. Atomic force microscopy analysis

Surface morphologies and roughness were also measured using the SPM-AFM system (Bruker/ Veeco/Digital Instruments NanoScope V). The images 5 μm by 5 μm were obtained using silicon AFM probe (RTESP-300, Bruker) in tapping mode at a resonance frequency between 200 kHz to 400 kHz. The 3D images and surface roughness were analyzed using NanoScope analysis software. The image was flattened using first order to remove the tilt in the line scan and adjust the image to the same average height.

3. Results

3.1. Weight loss

The total weight loss of disks was measured and the corrosion rate was calculated at 3, 15 and 30 days at 85 °C (see Fig. 1). The corrosion rate for the first 3 days was highest among all the conditions. The weight loss then decreased with the increase in immersion time. After 15 days, the corrosion rate approached a constant value, similar to that measured for 30 days. The total weight loss in pH 7 was within the error of the weight balance and therefore the results were not reported in this present study.

3.2. ICP analysis

The ions released into solution were measured by ICP and converted into the weight of the oxides. Fig. 2 demonstrates the weight of the released oxides in mg in basic and acidic conditions at 85 °C. Overall, the amount of released oxides was higher in an acidic than a basic environment, which was consistent with the corrosion results (Fig. 1).

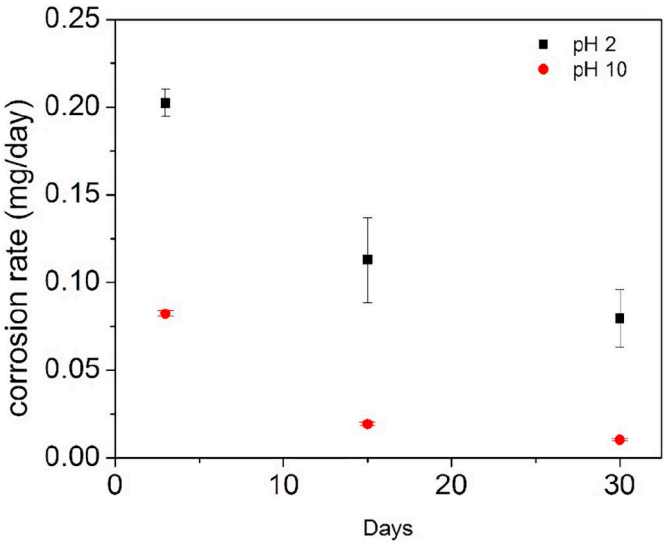

Fig. 1. The corrosion rate of disks in pH 10 and pH 2.

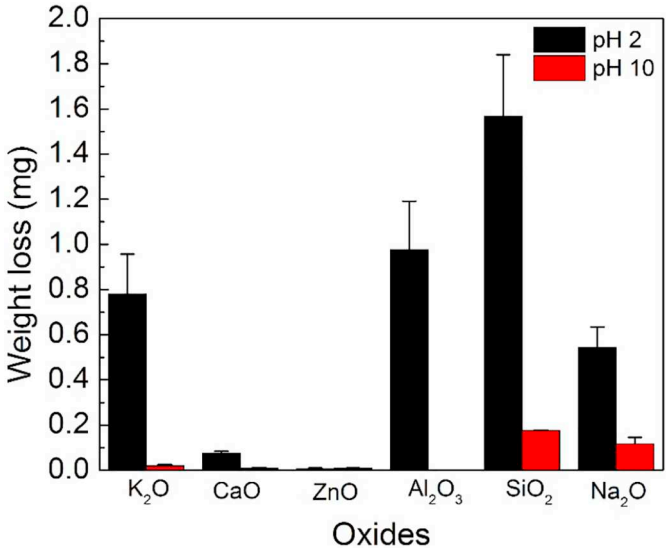

Fig. 2. Weight loss of individual oxide in pH 10 and pH 2.

The amount of oxides was released in the order of SiO_2 > Na_2O > K_2O > ZnO > CaO > Al_2O_3 in basic solution. In acidic solution the trend was SiO_2 > Al_2O_3 > K_2O > Na_2O > CaO > ZnO.

3.3. Dissolution activation energy

The activation energy was calculated for each oxide present in the glass-ceramic based on an Arrhenius Eq. (1);

$$LnW = \frac{-E_a}{RT} + lnA \quad (1)$$

where *W* is the corrosion rate, *Ea* is the activation energy, *R* is the gas constant as 8.314 J mol^{-1} K^{-1}, *T* is absolute temperature and *A* is the pre-exponential factor. The activation energy can be obtained by plotting natural logarithmic corrosion rates versus the inverse of absolute temperature. The representative plot is shown in Fig. 3. The slope of the regression line is the result of *-Ea/R*. The activation energies estimated for all the oxide components are listed in Table 2.

SiO_2 and ZnO had lower activation energies than the network modifiers, K_2O and Na_2O in basic solution. There were non-detectable concentration levels released for CaO and Al_2O_3 so their activation

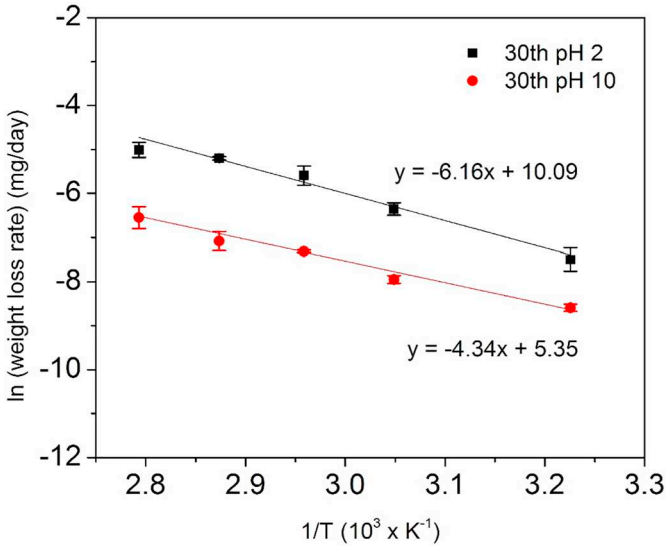

Fig. 3. Arrhenius plot of glass-ceramic dissolution in pH 10 and pH 2.

Table 2
The activation energy of individual oxide in pH 10 and pH 2, respectively.

Activation energy (kJ/mol)	CaO	K_2O	Na_2O	SiO_2	ZnO	Al_2O_3
pH 10	–	52.9	36.0	20.6	7.0	–
pH 2	28.5	58.8	44.8	70.5	28.0	50.5

Table 3
The activation energies in pH 10 and pH 2 based on the total weight loss and sum of weight percent of each individual oxide activation energy.

	Activation energy based on total weight (kJ/mol)	Sum of individual oxide (kJ/mol)
pH 10	30.42	26.53
pH 2	56.05	58.88

energies could not be calculated. However, in acidic solution, SiO_2 possessed the highest activation energy compared with K_2O, Na_2O and Al_2O_3. The activation energies for CaO and ZnO were similar.

The total weight loss of each disk was used to derive the activation energy based on Eq. (1), as shown in Table 3, to be 30.42 kJ/mol and 56.05 kJ/mol in pH 10 and for pH 2, respectively. The weight-loss based activation energy, E_{aw}, was also determined with the sum of individual oxide activation energies multiplied by the weight percentage of each individual oxide in the glass-ceramic;

$$E_{aw} = \Sigma\, E_{ai} \times f_o \quad (2)$$

where E_{ai} is the activation energy of individual ions and f_o is the weight fraction of a specific oxide corresponding to the individual released ion. Based on Eq. (2), the average activation energies obtained by the addition of the percentage weight of each individual oxide were 26.53 kJ/mol and 58.88 kJ/mol in pH 10 and for pH 2, respectively, as illustrated in Table 3.

3.4. Surface characterization

XRD was used to analyze the crystalline phases of glass-ceramic disks and the degree of crystallinity. The disks from before and after corrosion in 85 °C contained more than 94% ± 3% amorphous phase as given by the ratio between the area of the large amorphous bump located at around 2θ = 25° [20] and the whole areas under the diffraction peaks (Fig. 4a). The characteristic peaks identified the crystalline phase as Calcium Fluoride Phosphate, $Ca_5(PO_4)_3F$ and/or Calcium Fluoride Phosphate Hydroxide $Ca_5(PO_4)_3F_x(OH)_y$, where the patterns were closely matched to these two compounds. Fig. 4 shows the comparison of bulk patterns between each sample as well as the surface acquired patterns. The diffraction patterns acquired from bulk for each sample were almost indistinguishable. However, the surface region was less crystalline than the bulk for all samples. There was no secondary precipitate found in the corrosion areas.

The disks were also analyzed by XPS. Survey spectra acquired from samples are displayed in Fig. 5. Table 4 shows the atomic percentage of reference (non-corroded) and corroded disks. After immersion in pH 10 solution, the acquired spectra displayed less Na^+ and no K^+, P^+, Zn^{2+} and F^-, while after immersion in pH 2 solution the acquired spectra showed no Al^{3+}, Na^+, K^+, Ca^{2+}, Zn^{2+} and F^- but more P^{5+}.

The surface morphologies of the disks were examined under SEM (Fig. 6) and AFM (Fig. 7). The corroded disks demonstrated a different surface morphology than the reference disks. After exposure to pH 10 solution, the morphology showed generalized pitting on the surface. In contrast, there were isolated areas of pitting and roughness in pH 2 (Fig. 6). The surface roughness was analyzed using AFM. The corroded disks in pH 2 showed the roughest surface with R_q 563.2 ± 141.1 nm,

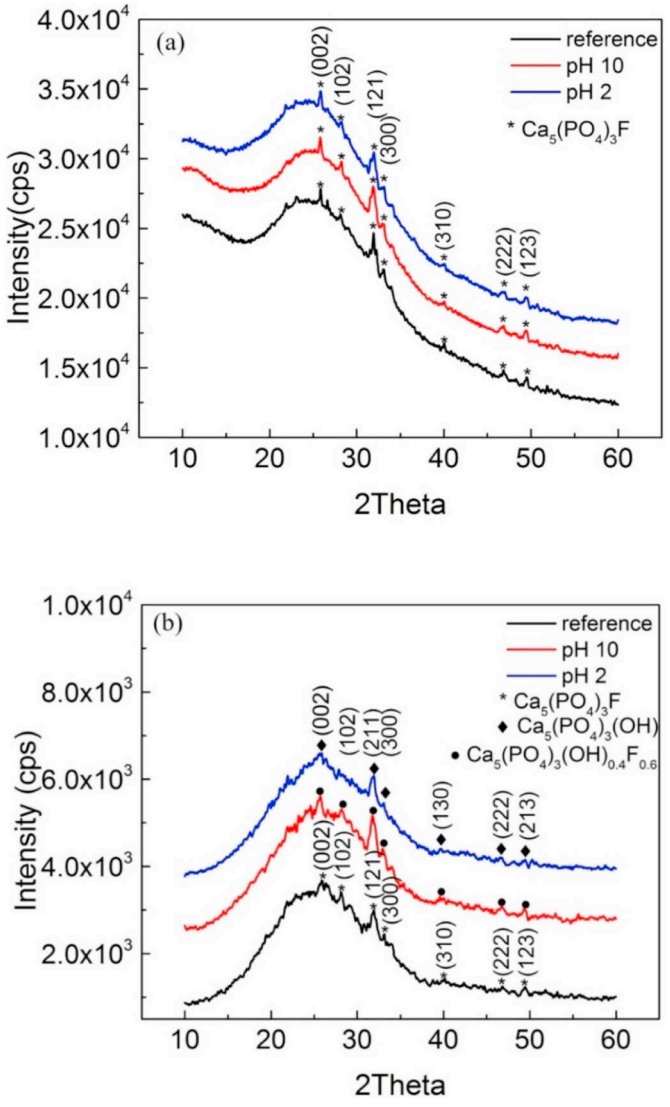

Fig. 4. XRD analysis of reference and corroded disks in pH 10 and pH 2 were shown in (a) bulk-symmetrical XRD and (b) surface-grazing incidence XRD.

followed by corroded disks in pH 10 with R_q 318.8 ± 40.5 nm and reference R_q 17.0 ± 4.3 nm.

4. Discussion

This study was undertaken to determine whether the use of an accelerated aging temperature to determine surface degradation of dental ceramics over an extended period of time is a reasonable assumption. That is, does an accelerated aging temperature elicit other reactions to occur which would not normally occur at 37 °C, the mouth temperature? The relationship between the weight loss rate of released oxides and temperature is shown in Fig. 3. The results were approximately linear where the glass-ceramic corrosion was accelerated with increasing temperature. This indicates that the corrosion at high temperatures or accelerated aging temperatures could be used to extrapolate longer time reactions at lower temperatures for this particular material. Based on Eq. (1), the slope of the data displayed in Fig. 3 was used to obtain the activation energy, which is presented in Table 2 as the activation energies of each oxide.

In an alkali environment, the activation energy of silicon dioxide was observed to be 20.6 kJ/mol (Table 2) which is in contrast with other studies that reported the activation energy of silica to be between 60.9 and 87.5 kJ/mol [1,3,18]. In general, an activation energy less than 20 kJ/mol indicates a diffusion-controlled process while an activation energy between 50 and 100 kJ/mol suggests the process is a surface reaction-controlled in liquid [21]. A possible explanation for the low activation energy observed for silica could be a hydrogen bonding effect at the interface between the glass-ceramic and the solution. During dissolution, the ionized surface of glass-ceramic contains SiO^- and NH_4^+ ions where a hydrogen bond could form with SiO^- [22]. This bond could prevent the diffusion of reagent (hydroxyl ions) from the solution to the surface or released ions from the surface to the solution. Non-bridging sites tend to attach to alkali ions more than H^+ in basic conditions resulting in higher activation energies for alkali oxides [23]. In addition, hydroxyl aluminates form in the base solution as Al(OH)x where x = 4, 5 or 6, and there was no detection of Al^{+3} ions in the solution. The hydroxyl aluminates usually absorb water molecules and swell up as a gel, which will further hinder $(OH)^-$ ions to diffuse into the SiO^- surface. This is consistent with the low activation energy of 20 kJ/mol for the diffusion-controlled glass-ceramic dissolution process.

In acidic conditions, the corrosion of glass-ceramic was favored through ionic exchange. Al^{3+} can be used as an intermediate ion replacing Si^{4+} in the glass-ceramic structure. In order to maintain a charge balance, univalent cations, such as Na^+ and K^+, are present in glass-ceramic. The equilibrium constant could be used to determine the extent of ion exchange. Bunker showed the ion exchange process was less in the presence of Al^{3+} [24]. This could explain the activation energies for K_2O, Na_2O and Al_2O_3. The leaching of K^+, Na^+ and Al^{3+} ions appeared to be reaction-controlled. CaO and ZnO were diffusion-controlled, whereby the leaching process was governed by mass transport [21,25]. While ions leach out, a hydrated surface can form on the surface of glass-ceramic. The dissolution of this hydrated surface becomes the rate-limiting step, which explains why SiO_2 had the highest activation energy (Table 2) in this environment.

Glass-ceramic based materials consist of network formers, intermediate ions and network modifiers. In a neutral condition or pH 7, there are two reactions that occur simultaneously to compete for the corrosion of glass-ceramic. The first reaction is a total dissolution process where the network former (or silica network), SiO_4, is broken down by hydroxyl ions. The second reaction is an ionic exchange reaction wherein the network modifiers, such as alkali metals or alkali earth metals, are released into solution through an exchange with hydrogen ions in solution. The M in the Eqs. (4) and (5) represents alkali metals or alkali earth metals.

$$-Si-O-Si-OH + OH^- = -Si-OH + -O-Si-OH \quad (3)$$

$$-Si-O-Si-OM + OH^- = -Si-OH + -O-Si-OM \quad (4)$$

$$-Si-O-M^+ + H^+ = -Si-OH + M^+ \quad (5)$$

Changes in pH of the environment are accompanied by different ion activities [26]. In an alkali environment, the activity of hydroxyl ions increases and favors the dissolution of silica network while the ionic exchange reaction is suppressed, preventing the leaching of network modifiers. In contrast, the activity of hydroxyl ions decreases in acidic conditions, while the activity of hydrogen ions for ionic exchange is favored.

The results of this study finding a lower release of SiO_2 in pH 10 is in contrast with other studies, where the dissolution of silica network is increased in basic conditions [6,27]. The silica network typically undergoes nucleophilic attack by hydroxyl groups and the Si-O-Si bond in the intermediate compound that is formed is cleaved [24]. This study demonstrates that glass-ceramic corrosion is not only related to structure and composition but also to the ionic composition of the environment [3,24,26,28,29]. According to earlier studies [28,29], NH_4OH, present in the pH 10 solution, demonstrated less corrosive

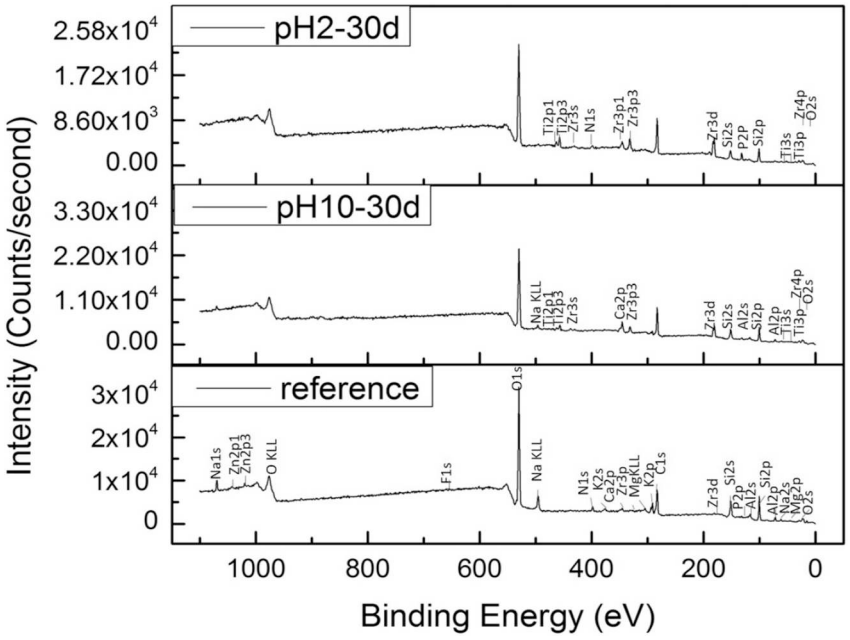

Fig. 5. XPS survey spectra acquired from reference (non-corroded) and corroded disks in pH 10 and pH 2 after 30 days.

Table 4
The atomic composition of reference (non-corroded), and corroded disks obtained from XPS survey spectra. C1s due to surface contamination was excluded from these estimations.

Atomic% (max-min)	Si	Al	Na	N	K	Ca	Mg	P	Zn	Zr	F	Ti
Reference	55.5–51.7	14.5–8.5	10.1–4.7	12.8–7.9	6.7–5.2	4.7–2.2	5.7–1.9	2.4–0.4	1.7–0.8	0.8–0.4	0.8–0.4	
pH 10	58.6	12.1	5.6			11.6				8.1		4.0
pH 2	49.4			11.7				16.7		13.3		8.9

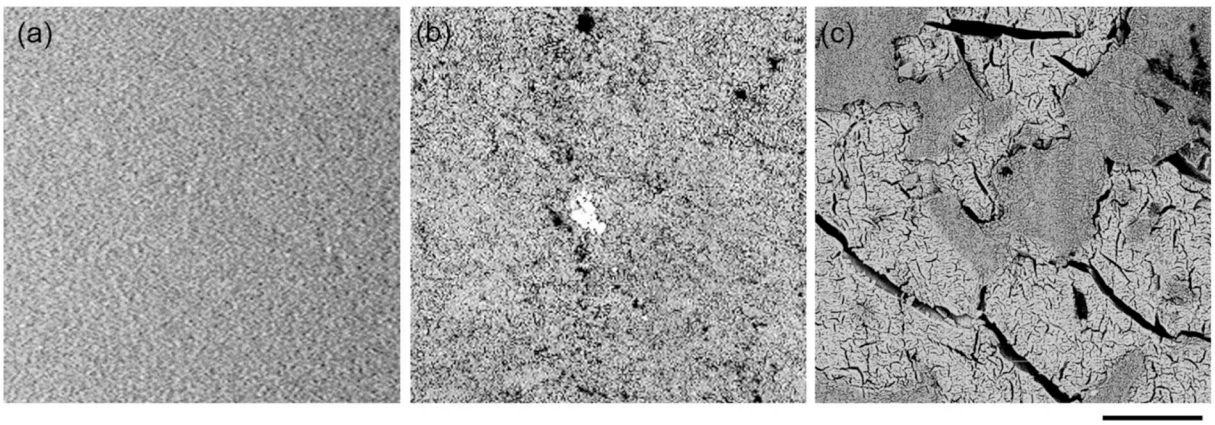

Fig. 6. SEM images of (a) reference (non-corroded), and corroded disks in (b) pH 10 and (c) pH 2 after 30 days. Scale bar: 30 μm.

ability compared with other solutions. This could explain why the dissolution of ions was a lot less in the basic environment for this experiment (Figs. 1 and 2).

Silicon dioxide, alumina dioxide, alkali metal and alkali earth metal oxides were released more in acidic than in basic conditions (Figs. 1 and 2). A previous study discussed five characteristics of glass surfaces in solution [30]: (1) the reacted surface has similar compositions as the bulk, and when conducted under neutral pH no significant material loss is observed; (2) a silica-rich surface is produced because of the lower alkali concentrations in the bulk and selective dealkalization reactions; (3) a silica-rich surface is also formed with fast dealkalization reactions or total network dissolution; (4) the reacted surface has a similar composition as the bulk but with substantial material loss due to uniform attack; and (5) protective layers are formed on the surface. They theorized that by introducing alumina oxide or calcium phosphate to a glass composition, a protective film could form on the glass surface, preventing surface reactions. In the present study, a silica-rich layer seemed to form on the surface and there were less alkali ions. These alkali ions may have gone through dealkalization reactions (Fig. 5 and Table 4).

In addition, other studies determined that non-bridging oxygen can attach to alkali metals/alkali earth metal instead of to H^+ in basic conditions, and silanol in acidic conditions [23]. This is another possible explanation for the non-detectable or very minimal release of CaO and Al_2O_3 as well as other oxides in the basic solution.

SEM and AFM results showed that disks corroded in pH 2 had the

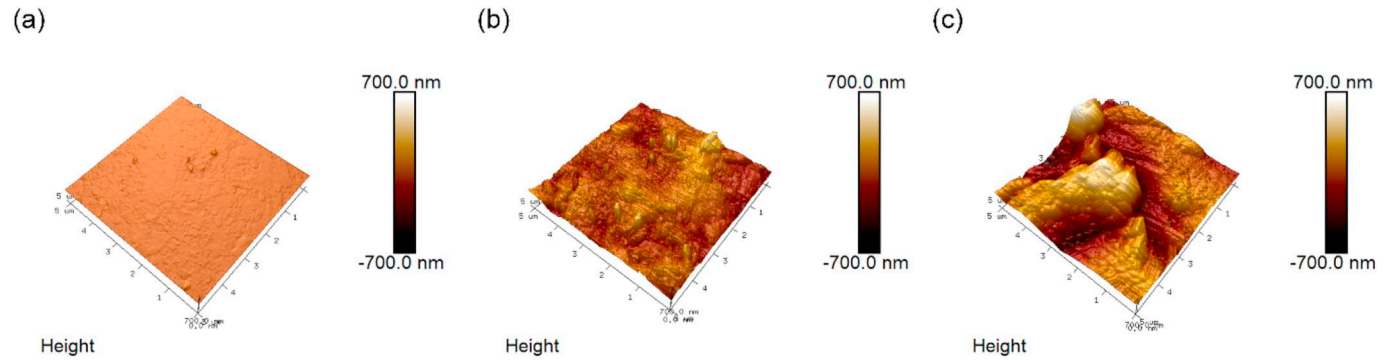

Fig. 7. AFM images of (a) reference (non-corroded), and corroded disks in (b) pH 10 and (c) pH 2 after 30 days.

roughest surface morphologies compared with disks corroded in pH 10 and reference disks (Figs. 6 and 7). This result coincides with weight loss results where the corroded disks in pH 2 demonstrated the highest weight loss (Figs. 1 and 2) compared with the other groups. The surface morphology for disks corroded in pH 2 demonstrated isolated areas of pitting and roughness, which is further evidence for the ion exchange mechanism that occurs in this environment [27]. The corroded disks in pH 10 had less rough surfaces with generalized pitting compared with the disks corroded in pH 2 (Figs. 6 and 7), which could be attributed to the less corrosive ability of NH_4OH pH 10.

XRD was performed to determine the crystal phase in glass-ceramic and whether a new secondary phase developed after corrosion (Fig. 4). The crystal phases of fluoroapatite glass-ceramic samples used in this study were identified as Calcium Fluoride Phosphate, $Ca_5(PO_4)_3F$ and/or Calcium Fluoride Phosphate Hydroxide $Ca_5(PO_4)_3F_x(OH)_y$ phases. The amount of crystalline phase was less than 6% ± 3% from Bragg-Brentano geometry analysis (Fig. 4a). Although the XRD pattern of the glass-ceramic disks in this study was close to both crystalline patterns, the non-corroded (reference) disk was considered to be Calcium Fluoride Phosphate. The non-corroded fluoroapatite glass-ceramic was obtained through sintering or heat treatment and would therefore not have any of the OH groups [31].

The surface of the reference disk was shown to be more amorphous than the bulk by grazing incidence X-ray diffraction geometry (Fig. 4). This could be the result of mechanical treatment with the diamond saw and sand paper polishing on the surface during sample preparation. For the corroded disks, the surface of the sample immersed in pH 10 appeared to be more crystalline than those immersed in pH 2 and reference samples (Fig. 4b). This increased crystallinity could be the result of a decrease in the area of the amorphous phase from dissolution reactions leading to a stronger signal to register compared with the original pattern. On the other hand, the surface of the sample immersed in pH 2 seemed to be less crystalline. This may indicate that the crystal phases went through a dissolution process. The peak around $2\theta = 28^{\circ}$ was diminished. There was no secondary phase found after corrosion.

The samples were also analyzed by XPS (Fig. 5 and Table 4) and showed that F^- was not detected in the corroded samples. The F^- and OH^- ions possibly underwent an ionic exchange, which corresponds with the Calcium (Fluoride) Phosphate Hydroxide $Ca_5(PO_4)_3F_x(OH)_y$ found in the XRD results. The percentage of phosphorus was higher but Ca^{2+} was less in disks corroded in pH 2 compared with reference disks. The formation of a P-enriched layer could be the result of an ionic exchange between Ca^{2+} and H^+, and OH^- and F^- [32]. On the other hand, P^{5+} was not detected in pH 10 but relatively higher Ca^{2+} levels were, which could indicate that the phosphorus ions are released through a dissolution mechanism [33].

The samples used in this study were a mixture of crystalline materials and glass. The crystal phase was less than 6% ± 3% and was identified as $Ca_5(PO_4)_3(OH)/F$. Therefore, this material was more than 95% of an amorphous glassy phase. There was difficulty in determining whether the dissolved Ca^{2+} and P^{5+} ions originated from the crystal or glassy phase since both these ions were present in both phases. The dissolution of SiO_2 in alkali conditions was a diffusion-controlled process resulting from the presence of hydrogen bonds, and was reaction-controlled under acidic conditions. The dissolution of K_2O, Na_2O and Al_2O_3 seemed to be reaction-controlled, whereas CaO and ZnO were governed by mass transport. The overall activation energy of glass-ceramic can be obtained from total weight loss of glass-ceramic as well as the sum of individual oxide activation times the weight fraction of individual released oxide in the glass-ceramic.

5. Conclusions

The activation energy for aqueous dissolution of a glass-ceramic veneer was calculated using ion release data during corrosion at different pH environments and temperatures. The activation energies derived over several temperatures demonstrated a linear trend which justifies the use of increased temperatures for accelerated aging reactions for this particular material. This study also found the composition of this fluorapatite glass-ceramic veneer to be 95% amorphous glassy phase and identified $Ca_5(PO_4)_3(OH)/F$ as the crystalline phase. In comparison with other studies [1,3,18], the dissolution activation energy of silicon dioxide was observed to be 20.6 kJ/mol under a diffusion-controlled alkali condition owning to the composition of the particular buffer solution. This work is expected to provide a better understanding of the performance of fluoroapatite glass-ceramic dental veneer material in the oral environment. Future work should include investigation of other materials that are subjected to accelerated aging to determine whether the use of this testing methodology is warranted.

Declaration of competing interest

There are no conflicts of interest associated with this research project.

Acknowledgements

NIH-NIDCR Grant R01 DE025001 supported this study. Ceramic materials were supplied by Ivoclar Vivadent. XPS was performed in Nanoscale Research Facility in University of Florida. XRD analysis was partially funded by NUCLEU –INFLPR project. We acknowledge Yuan Lin and Kimberly Beers for their significant contributions to this project.

There are no conflicts of interest associated with this research project.

References

[1] J.D. Rimstidt, H.L. Barnes, The kinetics of silica- water reactions, Geochim. Cosmochim. Acta 44 (11) (1980) 1683–1699.

[2] J.J. Mazer, J.V. Walther, Dissolution kinetics of silica glass as a function of pH between 40 and 85°C, J. Non-Cryst. Solids 170 (1) (1994) 32–45.
[3] H. Maraghechi, F. Rajabipour, C.G. Pantano, W.D. Burgos, Effect of calcium on dissolution and precipitation reactions of amorphous silica at high alkalinity, Cem. Concr. Res. 87 (2016) 1–13.
[4] M. Montazerian, E.D. Zanotto, Bioactive and inert dental glass-ceramics, J. Biomed. Mater. Res. A 105 (2) (2017) 619–639.
[5] M. Herrmann, Corrosion of silicon nitride materials in aqueous solutions, J. Am. Ceram. Soc. 96 (10) (2013) 3009–3022.
[6] J.F. Esquivel-Upshaw, F. Ren, S.M. Hsu, F.Y. Dieng, D. Neal, A.E. Clark, Novel testing for corrosion of glass-ceramics for dental applications, J. Dent. Res. 97 (3) (2018) 296–302.
[7] M.A. Bridges, M.R. Mattice, Over two thousand estimations of the ph of representative foods*, Am J Dig Dis 6 (7) (1939) 440–449.
[8] P. Jain, P. Nihill, J. Sobkowski, A. MZ, Commercial soft drinks: pH and in vitro dissolution of enamel, Gen. Dent. 55 (2007) 150–154.
[9] A. Lussi, B. Megert, R. Peter Shellis, X. Wang, Analysis of the erosive effect of different dietary substances and medications, Br. J. Nutr. 107 (2) (2012) 252–262.
[10] J.H. Meurman, J. Toskala, P. Nuutinen, E. Klemetti, Oral and Dental Manifestations in Gastroesoph-ageal Reflux Disease. *Oral Surgery, Oral Medicine, Oral Pathology, and Oral Radiology*, 78 (1994), pp. 583–589.
[11] W.K. Seow, K.M. Thong, Erosive effects of common beverages on extracted premolar teeth, Aust. Dent. J. 50 (3) (2005) 173–178.
[12] K.J. Anusavice, Degradability of dental ceramic, Adv. Dent. Res. 6 (1992) 82–89.
[13] M.M. Pinto, P.F. Cesar, V. Rosa, H.N. Yoshimura, Influence of pH on slow crack growth of dental porcelains, Dent. Mater. 24 (6) (2008) 814–823.
[14] S. Štefančić, L. Ćurković, G. Baršić, M. Majić-Renjo, K. Mehulić, Investigation of glazed Y-TZP dental ceramics corrosion by surface roughness measurement, Acta Stomatol. Croat. 47 (2) (2013) 163–168.
[15] M. Ghazal, M. Kern, The influence of antagonistic surface roughness on the wear of human enamel and nanofilled composite resin artificial teeth, J. Prosthet. Dent. 101 (5) (2009) 342–349.
[16] W. Teughels, N. Van Assche, I. Sliepen, M. Quirynen, Effect of material characteristics and/or surface topography on biofilm development, Clin. Oral Implants Res. 17 (S2) (2006) 68–81.
[17] K. Kawai, M. Urano, S. Ebisu, Effect of surface roughness of porcelain on adhesion of bacteria and their synthesizing glucans, J. Prosthet. Dent. 83 (6) (2000) 664–667.
[18] S.T. Bashir, L. Yang, J.J. Liggat, J.L. Thomason, Kinetics of dissolution of glass fibre in hot alkaline solution, J. Mater. Sci. 53 (2018) 1710–1722.
[19] IPS e.max zirpress scientific documentation; (Ivoclar vivadent).
[20] H.C. Li, D.G. Wang, J.H. Hu, C.Z. Chen, Effect of various additives on microstructure, mechanical properties, and in vitro bioactivity of sodium oxide-calcium oxide-silica-phosphorus pentoxide glass–ceramics, J. Colloid Interface Sci. 405 (2013) 296–304.
[21] T. Yoshida, Leaching of zinc oxide in acidic solution, Mater. Trans. 44 (2003) 2489–2493.
[22] P.M. Dove, J. Icenhower, Kinetic and thermodynamic controls on silica reactivity: an analog for waste disposal media. In *CEA/Valrho Summer Session Glass scientific Research for High Performance Containment*, France, 1997.
[23] B.C. Bunker, D.R. Tallant, T.J. Headley, G.L. Turner, R.J. Kirkpatrick, The structure of leached sodium borosilicate glass, Phys. Chem. Glasses 29 (3) (1988) 106–120.
[24] B.C. Bunker, Molecular mechanisms for corrosion of silica and silicate glasses, J. Non-Cryst. Solids 179 (1994) 300–308.
[25] M. Kukizaki, T. Nakashima, Acid leaching process in the preparation of porous glass membranes from phase-separated glass in the Na_2O-CaO-MgO-Al_2O_3-Ba_2O_3-SiO_2 system, Membrane 29 (5) (2004) 301–308.
[26] R.W. Douglas, T.M.M. El-Shamy, Reactions of glasses with aqueous solutions, J. Am. Ceram. Soc. 50 (1967) 1–8.
[27] J.F. Esquivel-Upshaw, F.Y. Dieng, A.E. Clark, D. Neal, K.J. Anusavice, Surface degradation of dental ceramics as a function of environmental pH, J. Dent. Res. 92 (5) (2013) 467–471.
[28] V.S. Molchanov, N.E. Prikhid'ko, Corrosion of silicate glasses by alkaline solutions communication 4. Corrosion of glasses by solutions of various hydroxides, Russ. Chem. Bull. 7 (8) (1958) 893–897.
[29] D. Hubbard, G.F. Rynders, Voltage anomalies of the glass electrode and the chemical durability of the glass, J. Res. Natl. Bur. Stand. 39 (1947) 561–570.
[30] L.L. Hench, D.E. Clark, Physical chemistry of glass surfaces, J. Non-Cryst. Solids 28 (1978) 83–105.
[31] C. Ritzberger, M. Schweiger, W. Höland, Principles of crystal phase formation in Ivoclar Vivadent glass-ceramics for dental restorations, J. Non-Cryst. Solids 432 (2016) 137–142.
[32] Y. Zhu, X. Zhang, Y. Chen, Q. Xie, J. Lan, M. Qian, N. He, A comparative study on the dissolution and solubility of hydroxylapatite and fluorapatite at 25 °C and 45 °C, Chem. Geol. 268 (1) (2009) 89–96.
[33] C. Chaïrat, E.H. Oelkers, J. Schott, J.-E. Lartigue, Fluorapatite surface composition in aqueous solution deduced from potentiometric, electrokinetic, and solubility measurements, and spectroscopic observations, Geochim. Cosmochim. Acta 71 (24) (2007) 5888–5900.